ELSEVIER

Journal of Nuclear Materials 254 (1998) 22–33

journal of nuclear materials

Fission product release from trace irradiated UO_{2+x}

M.A. Mansouri, D.R. Olander *

Department of Nuclear Engineering, University of California, Berkeley, CA 94720, USA

Received 19 August 1997; accepted 11 November 1997

Abstract

Fission-product release experiments were performed on trace-irradiated specimens of LWR fuel. The behavior of Te, I, Ru, Mo and Xe were followed in stoichiometric and pre-oxidized fuel. Maintenance of the desired O/U ratio was accomplished using an in situ microbalance during annealing. Fractional releases were determined from the intensities of characteristic gamma rays of the five fission product elements. Release fractions increased linearly with the square root of anneal time and decreased slightly as the specimen thickness was increased. No theoretical model could account for the effects of these two observations simultaneously. Comparison of the appropriately time- and size-scaled release data showed modest effects of oxidation on release kinetics, with Mo and Ru being most affected. Arrhenius plots exhibited breaks in linearity in the oxidized specimens, and the activation energies of the high-temperature portions were larger than commonly observed. Release during experiments in which oxidation (by steam) took place during annealing showed practically no dependence on temperature and were systematically higher than the release fractions measured during comparable constant-stoichiometry tests. © 1998 Elsevier Science B.V.

1. Introduction

Fuel oxidation by steam occurs in normal operation of a defective fuel rod and during a severe accident. One of the principal consequences of the conversion of UO_2 to UO_{2+x} is an increase in the diffusion coefficient of the fission gases and probably of many other fission products as well. The literature contains contradictory measurements of Lindner and Matzke (L&M) [1] and Miekeley and Felix (M&F) [2] on the stoichiometry effect on rare gas mobility. Both of these studies utilized powdered fuel specimens to avoid grain boundary effects. The L&M results show a pronounced dependence of xenon diffusivity on x in UO_{2+x}. The M&F data revealed that xenon diffusion in stoichiometric material is significantly lower than that in the hyperstoichiometric oxide, but the latter does not depend on x. Matzke [3] discusses the drawbacks of these experiments, some of which are due simply to their relative antiquity.

Current mechanistic fuel behavior modeling [4] treats fuel stoichiometry effects on fission gas release using the model advanced by Killeen and Turnbull (K&T) [5]. The model is consistent with the L&M data in the sense that the predicted diffusion coefficient increases with increasing x. In the range investigated by L&M ($1000 < T < 1300$ K; $0.005 < x < 0.12$), the xenon diffusion coefficient is given approximately by

$$D^{\mathrm{exp}}_{\mathrm{L\&M}}\left(\mathrm{cm}^2/\mathrm{s}\right) = 7 \times 10^{-5} \mathrm{e}^{-52/RT} x^{1.3}.$$

For the same conditions, the K&T model simplifies to

$$D^{\mathrm{theor}}_{\mathrm{K\&T}}\left(\mathrm{cm}^2/\mathrm{s}\right) = 9 \times 10^{-3} \mathrm{e}^{-60/RT} x^{2}.$$

The two diffusivity expressions are in good agreement for $x = 0.12$, but because of the different exponents on the stoichiometry excess, differ by about an order of magnitude at $x = 0.005$.

The present study seeks to resolve this unsatisfactory situation by introducing several improvements over the older experiments. First, sintered specimens cut from actual fuel pellets are used rather than fine powder. Although this change renders the solid medium more representative

* Corresponding author. Tel.: +1-510 642 5010; fax: +1-510 643 9685.

0022-3115/98/$19.00 © 1998 Elsevier Science B.V. All rights reserved.
PII S0022-3115(97)00350-4

of real fuel, it introduces the complication of grain growth during fission gas release. This additional factor is not important in stoichiometric UO_2, where the temperature at which rapid grain growth starts ($\sim$ 1900°C) is above the range in which release is measured (1200–1700°C). In UO_{2+x}, however, the greatly enhanced uranium ion diffusivity that accompanies hyperstoichiometry [1] produces grain growth at much lower temperature than in $UO_{2.00}$. The second experimental improvement is to establish the stoichiometry by steam oxidation(either prior to or during the gas release anneal) and assure its maintenance during the anneal by an in situ microbalance. The third feature of the present experiments is the measurement of the release properties of fission products other than Xe and Kr. The experimental problem of determining release of reactive volatiles such as I and Te is the difficulty of transporting them from the hot specimen to the radiation detector while avoiding loss on metal surfaces of the apparatus. This problem is avoided in the present method by measuring the fission product gamma-ray spectra of the specimen before and after the release anneal. This technique was developed by Prussin and co-workers [6,7] for similar measurements on stoichiometric UO_2.

The objective of the present work is to improve understanding of the transport properties of several fission products from UO_2 specimens with a simple microstructure in closely-controlled environments. In particular, the trace-irradiated fuel is not representative of the commercial high-burnup fuel, in which fission product release kinetics are determined by processes not active in fresh fuel. However, certain phenomena are common to trace- and highly-irradiated fuel (e.g., lattice diffusion of fission products), so the results of this study will have an indirect bearing on the performance of LWR fuel at high burnup.

2. Experimental

Fig. 1 shows the furnace used to anneal irradiated UO_{2+x} specimens for the fission-product release experiments. The specimen is hung in the hot zone of the alumina furnace tube from the arm of a continuously-recording microbalance. The temperature ranges from 1200 to 1700°C. Gas flow is provided by an H_2/He mixture, whose composition is chosen to maintain the preset stoichiometry of the sample during annealing. The O/U ratio is preserved by flowing He/H_2 gas mixtures with the following percentages of hydrogen: 4% for $UO_{2.00}$; 0.03% for $UO_{2.08}$; and pure He for $UO_{2.20}$. The concentrations of H_2 were determined from experience and served to counteract the oxidizing tendency of impurity water vapor in the He supply and of oxygen-containing gases desorbed from the internals of the apparatus in contact with the flowing helium. Because of noise in the microbalance signal, the smallest detectable change in O/U is $\sim$ 0.002. The 4% H_2 in He gas preserves exact-stoichiometry UO_2 to a much higher accuracy than the microbalance can detect.

The specimens are 8.7 mm diameter UO_2 disks with thicknesses ranging from 0.4 to 1.5 mm that had been cut from commercial fuel pellets. The open and closed porosities were measured to be 1% and 4%, respectively. The average grain size of the as-fabricated specimens is 8 μm. The initial oxidation state of the specimen is fixed by passing pure steam from a boiler through the furnace at 1200°C and stopping oxidation when the specimen weight gain corresponds to the desired O/U ratio. To prepare $UO_{2.20}$, the contact time in steam is 5 h; for $UO_{2.08}$, about 2 h suffices. During this preparation process, essentially no grain growth occurs.

After the stoichiometry is established by the method outlined above, the disk is placed in a quartz vial, sealed in argon, and irradiated for $\sim$ 15 min in a thermal neutron flux of $\sim 3 \times 10^{12}$ cm^{-2} s^{-1} at a temperature $<$ 200°C. Irradiation is followed by a one-week cooling period. The burnup is 10^{-8} FIMA, which is just below the neutron dose at which trapping by radiation-produced defects begins to affect rare gas diffusion coefficients [8]. Also, the burnup used for the present tests is too low to develop (during annealing) the fission-gas bubble morphology characteristic of high-burnup reactor fuel. However, in the oxidized specimens, substantial grain growth occurs during annealing. Thus the fission product diffusion properties measured by this method represent intrinsic mobility in the UO_2 lattice and long-range transport by fast paths such as grain boundaries, dislocations, or porosity which are native to the as-fabricated oxide.

Fractional releases are determined by measuring with a germanium detector the areas under selected fission product gamma-ray peaks before and after annealing. For the irradiation and cooling times used, Xe, I, Ru, Te and Mo could be readily distinguished in the gamma ray spectrum but Cs could not. The accuracy of the measurements of the fractional release is basically due to peak-fitting errors and, excepting xenon, is of the order of 2–3%. Fractional releases less than this cannot be accurately measured.

Xenon measurement is at once the most important and the most difficult. The photopeak at 81 keV is noisy and the accuracy of the fractional release determination is poorer than for the other fission products. Therefore, for this fission product, provision was made to used the classic method of trapping the released xenon in the charcoal absorber shown in Fig. 1. This improves accuracy (because the result is no longer the difference between two large

[1] Because anion Frenkel defects predominate in urania, an increase in the oxygen interstitial concentration causes a drop in the oxygen vacancy concentration. By the secondary Schottky equilibrium, the uranium vacancy concentration increases, thereby elevating uranium mobility. This model is the basis of the K&T theory [5].

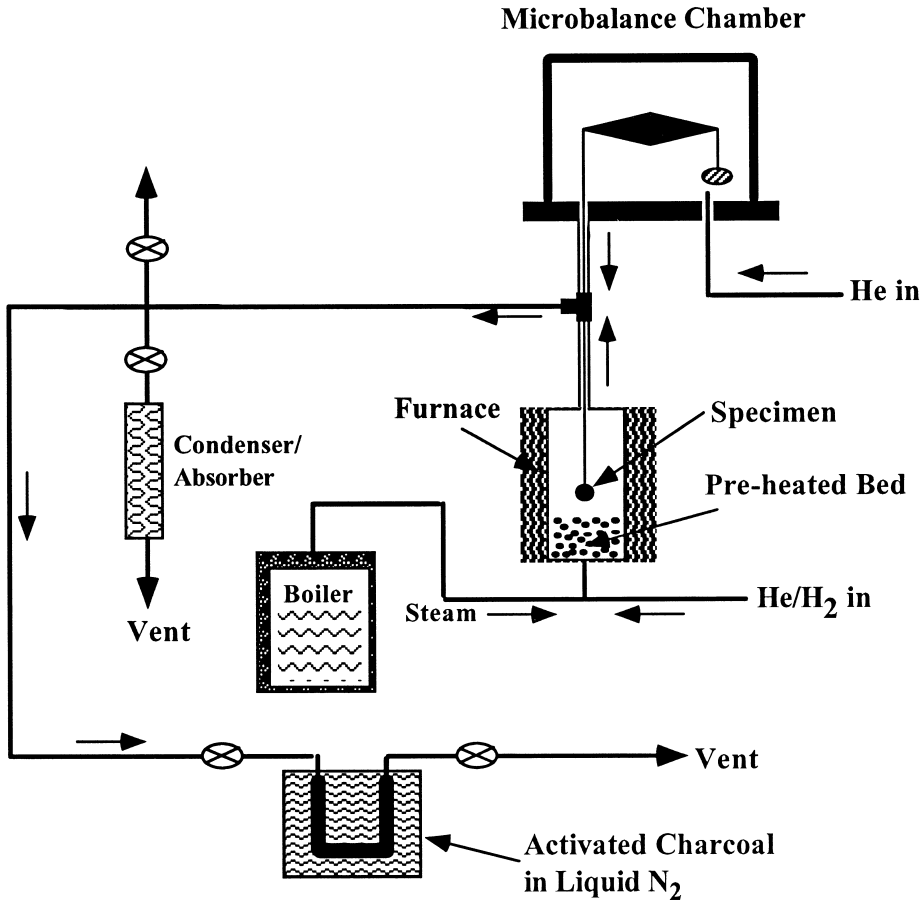

Fig. 1. Fission-product release apparatus.

numbers) but involves problems of detection geometry not encountered when the UO_2 disk is measured before and after annealing. These and other experimental details are discussed in Ref. [9].

The preceding description applies to anneals in which the fuel O/U ratio is held at a preset value. Tests were also performed in which the specimen oxidized during the anneal. For these experiments, stoichiometric UO_2 is irradiated and the anneals are conducted in a pure steam atmosphere. In these tests, oxidation and fission product release proceeded simultaneously.

3. Results and interpretation of the fixed-stoichiometry experiments

3.1. Grain growth

Although the increase in mean grain size during the <5 h exposure to 1200°C steam needed to establish specimen stoichiometry was negligible, considerable grain growth in the hyper-stoichiometric specimens is observed in the long-time anneals at high temperature. Grain growth kinetics in $UO_{2.08}$ and $UO_{2.20}$ were obtained from photomicrographs of polished and etched sections of annealed specimens using the mean-intercept method. Although a cubic law provides a somewhat better fit, the final grain diameters were reasonable well represented by the parabolic grain-growth law:

$$d^2 = d_0^2 + kt, \tag{1}$$

where d_0 is the initial grain diameter (8 μm) and d is the mean grain diameter after an anneal of time t. The grain growth constant in Eq. (1) depends on the O/U ratio according to

$$k = 0.6\exp(-39\,600/T) \quad \text{for } UO_{2.08}, \tag{2a}$$

$$k = 7\times10^{-3}\exp(-29\,700/T) \quad \text{for } UO_{2.20}. \tag{2b}$$

The unit of k is cm^2/s. The parabolic law is adopted to permit comparison of the data with theoretical models.

3.2. Fission product release

3.2.1. Release from stoichiometric UO_2

In agreement with the results of Prussin et al. [6,7], tellurium was found to be the most mobile fission product in stoichiometric UO_2 and xenon the least. Quantitative comparison of the present data for the 'volatile' fission products Te, I and Xe with those of Refs. [6,7] is accomplished via the effective diffusion coefficient (D/a^2) of the Booth model. D is the lattice diffusion coefficient of the fission product in the solid and a is the effective radius of the sphere in which transport occurs. In the Booth model, D and a cannot be independently determined from fraction release measurements alone. Reporting release measurements as effective diffusivities is equivalent to removal of the time-dependence of the fractional release by use of the formula

$$f = \frac{6}{\sqrt{\pi}}\left(\frac{Dt}{a^2}\right)^{1/2}, \tag{3}$$

where f is the fractional release in anneal time t. This equation is a short-time approximation to the exact solution. It is in error by 10% at $f = 0.31$ and by 12% at $f = 0.36$. Since all but a few of the measured fractional releases were less than 0.35, use of Eq. (3) to represent the data is considered to be adequate.

Using the data for release from stoichiometric UO_2 in Eq. (3) provides the effective diffusion coefficient D/a^2, whose temperature dependence is of the form

$$\frac{D}{a^2} = A\exp\left(-\frac{E}{RT}\right), \tag{4}$$

where A is the pre-exponential factor and E is the activation energy.

For tellurium in UO_2, the Arrhenius plot [$\log(D/a^2)$ vs. $1/T$] is reasonably linear and has approximately the same activation energy as the analogous plots in Refs. [6,7]. However, the pre-exponential factor from the present data for Te is slightly more than an order of magnitude lower than those associated with the Arrhenius plots for this element reported in Refs. [6,7].

Arrhenius behavior of D/a^2 is observed for xenon in the present study, with an activation energy close to that reported for this species in Refs. [6,7]. However, the pre-exponential factor from the current work is approximately two orders of magnitude smaller than those reported in the previous studies.

The large differences in the magnitudes of the effective diffusion coefficients of fission gas in nominally stoichiometric, trace-irradiated UO_2 in specimens of similar grain size are a common observation [10]. This extreme variability may be due to uncontrolled impurity levels in the specimens, to the creation of solute-trapping sites by irradiation [8], to pellet fabrication methods, or to stoichiometry control during the release anneals [3]. Previous studies of fission gas release did not employ the measures to control (and measure in situ) specimen stoichiometry during the release process. Use of 'pure' He as the carrier gas in previous experiments was shown in this work to cause slight oxidation during annealing, and probably did so in previous studies which did not have the facility to measure slight increases in fuel O/U. In the present study, addition of 4% H_2 to the helium carrier gas was necessary to prevent oxidation. The effective diffusivities reported in this investigation are believed to more faithfully represent fission product mobility in stoichiometric UO_2 than previous measurements. Maintenance of exact stoichiometry is probably the major reason that the measured effective diffusivities are one or two orders of magnitude lower than those previously reported.

That the Booth model is an oversimplification of the complexity of the fission-product release process has been recognized for decades. However, because of its extreme simplicity, it continues to be the gas-release model of choice in numerous fuel behavior codes. The inappropriateness of this model to describe the present data rests on two observations. First, for Te, which gives the largest and most accurate release fractions, f decreases with increasing specimen size. This dependence indicates the existence of a transport resistance due to a long-range diffusion process subsequent to lattice diffusion (or some other short-range process that acts on the scale of the size of a grain). Second, the magnitudes of the diffusion coefficients are too small to be explained solely by lattice diffusion in a sphere of the size of a grain. For example, when the release fraction for xenon after a 5 h anneal at 1400°C ($f = 0.0016$) is substituted into Eq. (3), a value of $D/a^2 = 1.2 \times 10^{-11}$ s^{-1} is obtained. If the radius of the Booth sphere is taken to be the grain radius (4 μm), the lattice diffusivity is 2×10^{-18} cm^2/s. This value is more than three orders of magnitude smaller than the frequently-cited value of 5×10^{-15} cm^2/s at this temperature [3,10]. To recover this diffusivity value from the present datum using the Booth model would require an effective sphere radius nearly one-third of the thickness of the specimen.

3.2.2. Release from hyperstoichiometric urania

In agreement with the observations of xenon release by L&M [1] and M&F [2], the present results show significant increases in fractional release from hyperstoichiometric specimens compared to stoichiometric samples, all other conditions being identical.

The most striking effect of oxidation on release is the reversal of the positions of the volatile elements Xe, I and Te and the 'low-volatile' elements Mo and Ru. In the hyper-stoichiometric state, the latter two elements exhibit the highest release fractions of the five element studied, whereas in the stoichiometric oxide, they were among the lowest. This reversal is attributed to the enhanced volatility of these elements due to the formation of the higher oxides

RuO_4 and MoO_3 on the free surfaces of the hyper-stoichiometric specimens. The relatively low release of Ru and Mo from stoichiometric UO_2 is due to the stability of the non-volatile elemental or lower-oxide states that these elements assume when the oxygen potential of the fuel is low. This surface chemical effect probably has a greater influence on release kinetics than the effect of the O/U ratio on the mobility of atomic Ru and Mo in the oxide lattice. The release fractions of Mo and Ru (unencumbered by volatility restraints) are considerably larger than those of Xe, Te and I. If interpreted in terms of the Booth model, this implies an order-of-magnitude difference in the lattice mobilities of these two fission product groups.

The speciation-dependent release rates of Ru and Mo observed in this study are characteristic of the low-volatile fission products, as described by Cubiocciotti [11] and incorporated into severe accident codes [12,13].

The release-rate enhancement in UO_{2+x} relative to that in UO_2 is attributed to one or both of the following mechanisms: increase in the concentration of cation vacancies by point-defect equilibria [5], which increases solute atom mobility in the lattice; and the substantial grain growth during annealing observed in the hyper-stoichiometric specimens, which supplements intragranular diffusion as a means of delivering solute to the grain boundaries.

3.3. Model-independent data analysis

Before examining the results in terms of mechanistic models, the data are reduced to a more manageable form. The release process depends on a number of variables, including:

- temperature,
- O/U ratio,
- fission product element,
- specimen thickness,
- anneal time.

In this section, the effects of variations of the last two experimental conditions in the database are empirically removed so that the influence of temperature can be expressed in Arrhenius form for the five species and three stoichiometries investigated.

3.3.1. Anneal time

The experiments involving Te, Ru, I and Mo release from $UO_{2.20}$ at 1600°C provide a systematic variation of specimen thickness (by a factor of three) at anneal times of five and nine hours. Examination of these data show that the release fractions for the two times reasonably well follow the square-root-of-time (root-t) law expected for a diffusion-controlled process (or processes) in finite media at short times. This behavior is assumed to apply to all results obtained in this study, and all data are scaled by the factor $\sqrt{10/t}$, where t is the anneal time in hours. Fig. 2 shows the results of applying this correction to the data at one temperature for each of the three stoichiometries investigated. For $UO_{2.20}$ at 1600°C, the pairs of points at the same specimen thicknesses are all within 10% of their average value despite nearly factor-of-two differences in anneal times. This good accord demonstrates the validity of the root-t scaling procedure.

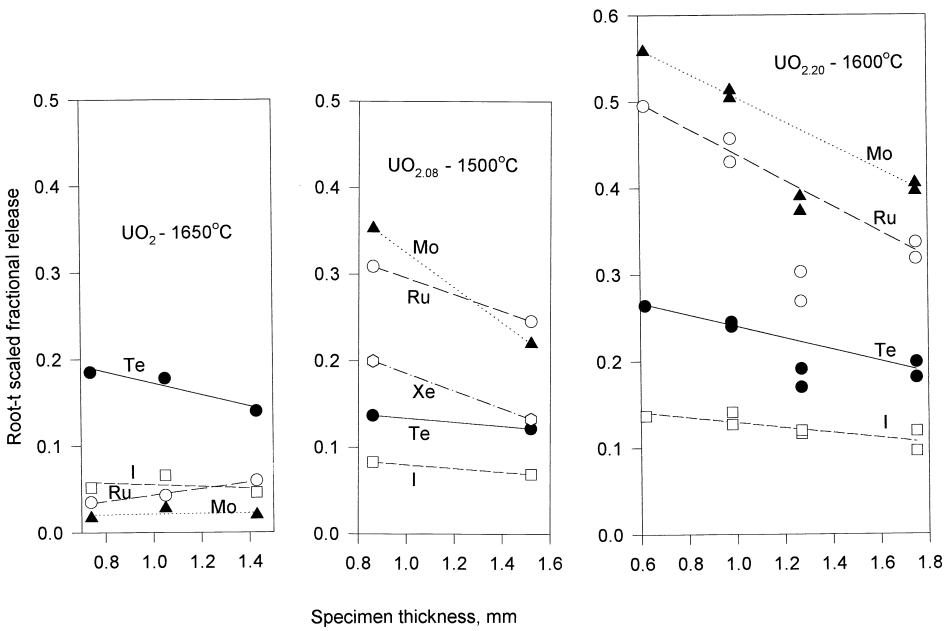

Fig. 2. Fractional releases scaled to 10 hour anneal time by the root-t law.

3.3.2. Specimen thickness

Fig. 2 also permits assessment of the effect of specimen thickness on the root-t scaled fractional releases. The three plots include tests at two or more specimen thicknesses. The fraction release decreases approximately linearly with specimen thickness except for a few cases with release fractions < 0.05 where data precision is poor. The slopes of these lines become smaller as the release magnitude increase, and the logarithmic derivatives:

$$\mathrm{LD} = \frac{\mathrm{d}\ln f}{\mathrm{d}\ln L} \cong \frac{L}{f}\frac{\Delta f}{\Delta L}, \tag{5}$$

where f is the fractional release and $2L$ is the specimen thickness, are approximately independent of the element released. The finite difference forms of the derivative are taken as the slopes of the lines on Fig. 2 and L and f in Eq. (5) are evaluated at the midpoint of the range of thicknesses. Table 1 gives the element-averaged logarithmic derivative,

$$\mathrm{LD}_{\mathrm{avg}} = \frac{1}{N}\sum_{i=1}^{N}(\mathrm{LD})_i, \tag{6}$$

where $(\mathrm{LD})_i$ is the logarithmic derivative of element i and N is the total number of elements included in the sum. The mean deviations from the averages are also given in the table.

All of the logarithmic derivatives are greater than zero, and except for $UO_{2.20}$ at 1550°C, are statistically less than unity. This observation can be compared to expected values of LD for limiting cases of transport models. For the Booth model, release is predicted to be independent of specimen thickness, or the logarithmic derivative as defined by Eq. (5) should be zero. This is clearly not shown by the results in Table 1.

The opposite theoretical limit represents the case of rapid intragranular release and complete control of release by the long-range diffusion process that follows solute release from the lattice. Long range transport refers to the mechanism responsible for movement of the fission products from the interior of the specimen to its surface. For short times, the release fraction controlled by the long-range mechanism, f_{LR}, is given by

$$f_{\mathrm{LR}} \propto \sqrt{\frac{D't}{L^2}}, \tag{7}$$

where D' is the diffusion coefficient characterizing the long range process.

Whatever the mechanism of the long range process, if it is the slow step, the logarithmic derivative of f_{LR} with respect to L is, from Eq. (7), $\mathrm{LD} = -1$. The information collected in Table 1 shows that this limiting situation does not apply to the experimental data. Instead, the implication of Table 1 is that short-range transport and the long-range transport step offer resistances of comparable magnitude.

Table 1
Effect of specimen thickness on root-t fractional releases. Logarithmic derivatives are averaged over all elements

T (°C)	O/U ratio		
	2.00	2.08	2.20
1400	–	-0.55 ± 0.23	-0.64 ± 0.08
1450	–	-0.39 ± 0.13	-0.71 ± 0.18
1500	–	-0.50 ± 0.22	-0.51 ± 0.29
1550	–	–	-0.95 ± 0.13
1600	–	–	-0.38 ± 0.02
1650	–0.28[a]	–	–

[a] Te only

3.3.3. Temperature and stoichiometry

Irrespective of the precise mechanism of release, the effect of temperature can be shown by Arrhenius plots of the root-t scaled fractional releases at a common specimen thickness, which is taken as 1 mm. The data for these temperature plots are taken from the straight lines in Fig. 2 (and the comparable figures for other temperatures) at the selected specimen thickness. These standardized release fractions are plotted in Arrhenius fashion in Fig. 3 for the three stoichiometries investigated. The same data are displayed in Fig. 4 to emphasize the effect of stoichiometry on release. The curves in this figure represent tendencies of the O/U effect, not data fits.

The most significant effects seen in these plots are:

(a) The proximity of the Ru and Mo release fractions at all stoichiometries.

(b) The reversal of the relative magnitudes of the release fractions of Te and the Ru, Mo pair upon oxidation of the fuel.

(c) The generally small effect of stoichiometry on all fission product release fractions once the O/U ratio departs from 2.00.

(d) The relative immobility of Xe and I in oxidized specimens compared to the remaining three species, which are generally considered to be less volatile than the first two elements.

(e) The breaks in the Arrhenius lines at temperatures between 1400 and 1500°C suggests the existence of two parallel release mechanisms that operate independently of the series processes that are needed to explain the specimen-thickness effect discussed earlier.

Xenon release fractions increase by approximately one order of magnitude as the O/U ratio departs from 2.00, but are roughly the same in $UO_{2.08}$ and $UO_{2.20}$. This result is in accord with the M&F results [2], but not with the measurements of L&M [1] nor with the K&T theoretical model [5].

For $UO_{2.00}$, all five elements exhibit normal Arrhenius behavior at all temperatures. For $UO_{2.08}$, a change in slope

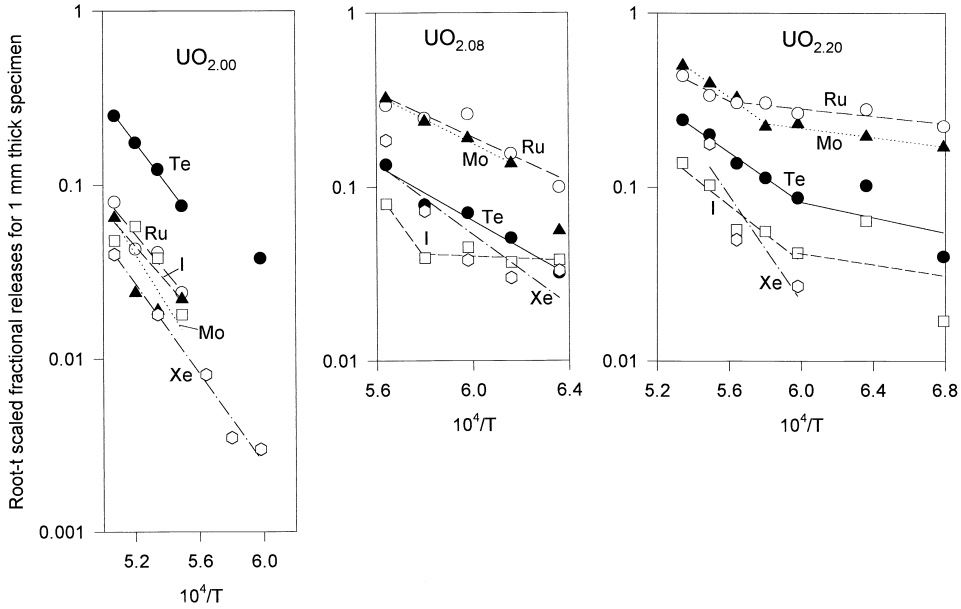

Fig. 3. Root-t scaled fractional releases from 1 mm thick specimens in 10 h anneals.

(break) of the Arrhenius plot for iodine appears at ~ 1450°C. In $UO_{2.20}$, all elements except perhaps Xe reveal breaks in the Arrhenius plots at temperatures between 1400 and 1500°C. The apparent activation energies of the high-temperature portions of the Arrhenius plots of Fig. 3 are summarized in Table 2.

In stoichiometric oxide, the activation energies of the standardized fractional releases are between 50 and 60

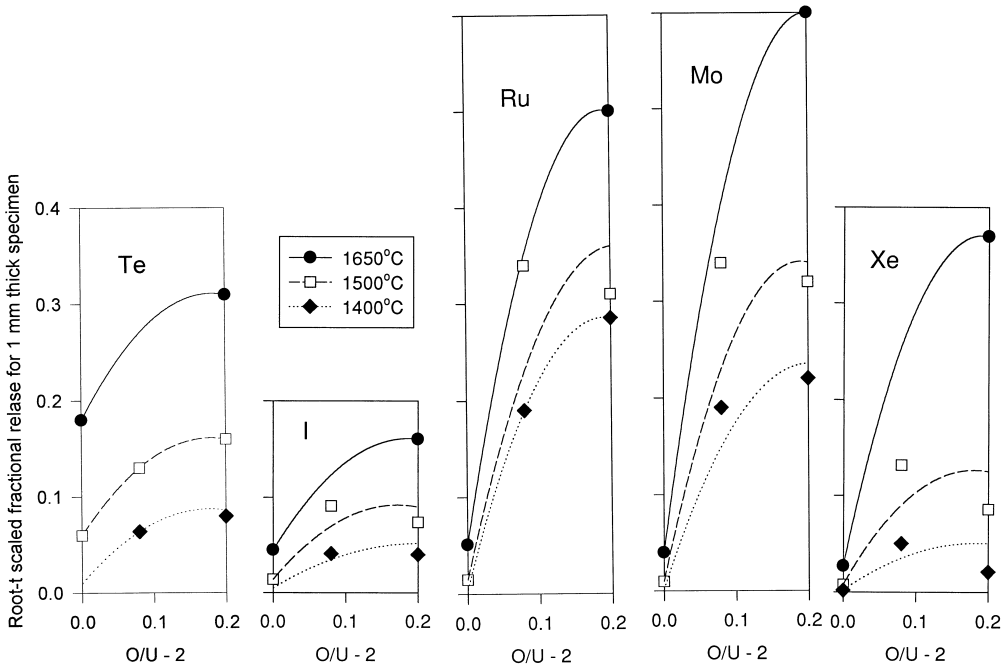

Fig. 4. Effect of O/U ratio on standardized fission product releases.

Table 2
Apparent activation energies (in kcal/mol) of the root-t scaled fractional releases from 1 mm thick specimens[a]

Species	O/U ratio		
	2.00	2.08	2.20
Mo	69	32	34(5)
Ru	52	29	23(6)
Te	56	36	33
I	48	89(3)	37
Xe	59	47	69

[a]Figures in parentheses are for temperatures below the breaks in the Arrhenius lines

kcal/mol. The high value for Mo is attributed to the very scattered results for this element in stoichiometric fuel. The high-temperature activation energies in UO_{2+x} are generally lower than those in stoichiometric oxide by 10–20 kcal/mol. The exceptions are iodine in $UO_{2.08}$ and Xe in $UO_{2.20}$. However, the anomalous activation energies for these cases are based on single data points and should not be regarded too seriously. The activation energies at low temperatures (below the breaks) for Ru and Mo in the most highly-oxidized specimens are between 5 and 6 kcal/mol, and appear to be reliably established experimentally. The activation energies given in Table 2 do not represent a well-defined physical mechanism. Rather, they result from the admixture of the short range release process and the subsequent long-range step that is implied by the magnitudes of the logarithmic derivatives of f with respect to L.

4. Mechanistic interpretations

The preceding section has provided two characteristics of the release kinetics that a theoretical model must reproduce: the root-t behavior; and the variation with specimen thickness that is intermediate between the Booth model (none) and rate control by a diffusion process that occurs between the specimen interior and the free surface ($f \propto L^{-1}$). Table 3 gives the potential short-range and long-range transport processes which in combination produce the characteristics of the overall release process. For any combination of a short-range process and a long-range process, the fractional release from the specimen, f, has two contributions:

$$f = f_{SR} - (1 - f_{LR}), \tag{8}$$

where f_{SR} is the fractional release from the urania matrix to the pathways by which long range transport takes place. The term $1 - f_{LR}$ represents the fraction of the initial fission product charge that has been released from the fuel matrix but remains in the long-range transport medium. In this section, the most likely combinations of a short-range process with a long-range process are examined to determine if the anneal-time and specimen thickness dependences of the release data can be explained.

Table 3
Short- and long-range transport processes for fission product release in trace-irradiated fuel

Short-range process	Long-range process
1S lattice diffusion	1L grain boundary diffusion
2S grain boundary sweeping	2L pipe (dislocation) diffusion
	3L pore diffusion

4.1. Release enhanced by grain boundary sweeping and grain boundary diffusion

Augmented transport of impurity elements in metals by diffusion along grain boundaries (the 1S/1L combination in Table 3) is a well-established phenomenon [14,15]. This combination of transport processes has also been invoked to explain enhanced fission product release from low-burnup UO_2 [16,17] [2]. The data to which this combination of short- and long-range processes can be applied are those obtained for release from stoichiometric urania, in which grain growth did not occur. The release data for each fission product were fitted by the theory given in Ref. [17] by choosing lattice and grain boundary diffusivities. However, the validity of this exercise is problematical; at each temperature, the two transport properties are determined from two or at most three data points for different specimen thicknesses.

The problem of too few data points for the number of parameters to be determined is largely resolved in hyper-stoichiometric urania. In $UO_{2.08}$ and $UO_{2.20}$, the mean grain size increased by factors of 2 to 5 during the release anneals. The consequence of such extensive grain growth is the change the dominant short-range release process from lattice diffusion (process 1S in Table 1) to grain boundary sweeping (process 2S). Since the kinetics of grain growth have been independently determined (Eqs. (2a) and (2b)), only one parameter at each temperature, the grain boundary diffusivity, needs to be determined by fitting the model to the data. The theory on which this model is based is given in Ref. [18]. Because of the rapid depletion of the lattice of fission product by grain boundary sweeping, f_{SR} in Eq. (8) is near unity, and hence $f \cong f_{LR}$. The release process is thus controlled entirely by diffusion in the grain boundaries. Since f_{LR} varies as $t^{1/2}$ and L^{-1} (see Eq. (7)), this model agrees with the observed root-t dependence of the fractional releases but does not

[2] At high burnup, intergranular bubbles act as traps for fission products so grain boundary release takes place via the network of interconnected porosity rather than by intergranular diffusion.

agree with the experimental dependence on specimen size, which is less strong than L^{-1}.

4.2. Dislocations as high-diffusivity pathways

Although not as frequently applied as grain-boundary pathways, rapid diffusion along dislocations is known to accelerate solute transport in solids [19]. This mechanism is implicitly contained in the fission-gas behavior code ENIGMA, in which pipe diffusion appears in the guise of an apparent solubility of xenon in the fuel [20].

The lattice diffusion/dislocation diffusion mechanism (1S/2L in the notation of Table 3) is mathematically quite similar to the lattice diffusion/grain boundary diffusion combination (1S/1L) with one important physical difference. There is no analog of grain boundary sweeping in the dislocation diffusion process. Except in an irradiation field which induces climb, dislocations are generally not as mobile as grain boundaries. Even if dislocations were to move, they would 'sweep' only two-dimensional internal surfaces but could not collect solute from volumes of solid.

In order to assess the applicability of this model to the present data, the dislocation structure is assumed to consist of a regular array of stationary parallel lines that are all perpendicular to the specimen surface. This geometry permits restriction of the analysis to a unit cell consisting of a straight, infinite dislocation line centrally placed in a cylindrical annulus whose outer radius is fixed by the dislocation density. The dislocation line is assumed to be a black sink for solute diffusing to it. Fission product diffuses in the annular zone of crystalline urania (short-range process) and then along the dislocations to the free surface (long-range process). This model is developed in detail in Ref. [9]. It is found that the chief resistance to release of the fission product is lattice diffusion, with pipe diffusion relatively rapid. An approximate analytical representation of the predictions of the model is

$$f \cong Kt - K'L^2, \tag{9}$$

where, in the notation of Eq. (8), Kt is an empirical approximation to the release fraction f_{SR} and $K'L^2$ is an empirical approximation to $1 - f_{LR}$. The second term in Eq. (9) is small compared to the first term, but serves to reproduce the modest specimen-thickness effect seen in the right hand panel of Fig. 2 for Te (the release data in Fig. 2 also plot in a roughly linear fashion against L^2 as well as against L). However, the first term in Eq. (9) is much larger than the second, so the observed root-t behavior is not predicted theoretically. The reason is that the dimensionless time Dt/X^2 is short enough for the root-t limit to apply if the characteristic distance X is the grain radius but is not sufficiently short if X is the radius of the dislocation line.

4.3. Transport in porosity

Transport in the pores or cracks in the fuel is used in at least one fission product release code [21]. In this code, transport occurs by a combination of diffusion in the gas filling the internal spaces and bulk flow driven by a total pressure gradient (Darcy flow). Because of the very low burnup of the specimens used in the present investigation, internal pressure buildup due to volatile fission products escaping from the matrix is not possible, so gas phase diffusion is the only credible mechanism.

Following the method utilized in the VICTORIA code [21], fission products diffuse in the lattice to the grain boundaries with diffusion coefficient D. Upon reaching the grain boundaries, the fission products are immediately transferred to open porosity. In this model, grain boundary diffusion is assumed to be rapid and grain boundary sweeping is neglected.

The fission product transport equation in the porosity is Fick's second law with a source term representing solute supply from the grains via the grain boundaries. The dimensionless form of this conservation equation shows that two parameters govern the relative importance of pore transport relative to intragranular transport. The first parameter is the ratio of the characteristic times of diffusion in the grains to diffusion in the pores:

$$\alpha = \frac{d^2/D}{L^2/D_g}, \tag{10}$$

where d is the grain diameter, D_g is the diffusivity of the fission product in the gas filling the pores, and L is the specimen thickness. The second parameter, related to the source term in the diffusion equation, is the ratio of the initial concentration of the fission product in the solid, c_0, to the concentration of the fill gas in the pores,

$$\beta = c_0/\varepsilon c_g, \tag{11}$$

where ε is the fractional open porosity and c_g is the fill-gas concentration, given by the ideal gas law.

Using typical values of the quantities in Eqs. (10) and (11) gives $\alpha \sim 10^7$ and $\beta \sim 10^{-3}$ For this combination of parameters, the theory predicts negligible buildup of fission product in the pores. Or, in terms of Eq. (8), $f_{LR} = 1$, and the release process is controlled entirely by the short-range step. Gas-phase diffusion in the open porosity is rapid compared to intragranular diffusion and hence cannot be responsible for the specimen-thickness dependence or for the generally low values of the observed fractional releases.

In high-burnup fuel, however, pore diffusion may not be negligible. At burnups six or seven orders of magnitude

larger than the trace irradiation used in the present experiments, the concentration of fission products in the lattice is correspondingly larger than in trace-irradiated fuel. In this case, α and β are of comparable magnitudes, and the open porosity can hold up fission products released from the grains and thereby reduce the fractional release from the fuel. This is the reason that pore transport is considered in VICTORIA [21].

5. Release during oxidation

A series of experiments were performed using irradiated stoichiometric specimens in flowing steam rather than in helium. The steam environment caused oxidation of the specimen to equilibrium O/U ratios close to 2.20 for temperatures between 1400 and 1600°C. With a few exceptions, oxidation occurred in times that were short compared to the times of the anneal for fission product release. Weight gains showed that the equilibrium O/U ratios were reached in $\sim$35 min at 1400°C and in $\sim$8 min at 1600°C.

A single pair of specimens, one thick (>1 mm) and the other thin (<1 mm), was used in all runs at each temperature. The specimen pair was irradiated as stoichiometric UO_2, the gamma-ray spectra of each measured, then annealed as a pair for measurement of fission product release. Following recording of the post-anneal gamma ray spectra, the two specimens were reduced to UO_2 and re-irradiated for use in the next anneal at a longer time. Three or four anneal times were tested at each temperature. The general trend of reduction in release fraction with increase in specimen thickness that was observed in the constant-stoichiometry experiments was confirmed in the variable-stoichiometry tests.

In order to eliminate the specimen thickness effect, fractional releases from hypothetical 1-mm thick specimens were calculated by linear interpolation from the data pairs at the same anneal time and temperature. Elimination of the specimen thickness effect permits examination of the time dependence of the release process. Fig. 5 shows the fractional releases plotted against the square root of anneal time. The releases of the first two (or three) times fall consistently on straight lines that, with the exception of the data at 1600°C, pass through the origin (the data set at 1500°C, not shown in Fig. 5, is similar to those at 1400, 1450 and 1550°C). The releases at the longest anneal time consistently fall beneath the extrapolated root-t lines. This phenomenon was not observed in the constant-stoichiometry tests with $UO_{2.20}$ where the anneal times were comparable to the $\sim$450 min duration of the longest tests in steam.

Because steam was the ambient gas in the variable-stoichiometry tests, volatilization of the oxide occurred and augmented fission product release. Fuel evaporates as UO_3 at rates that were measured by the weight losses that

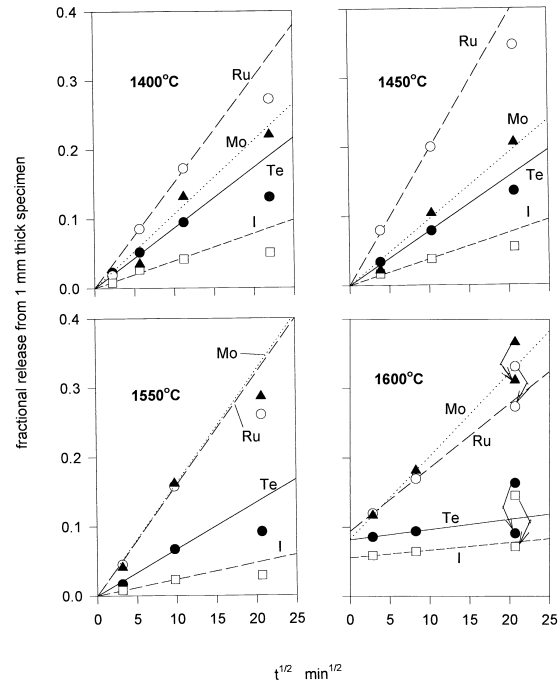

Fig. 5. Fractional releases from 1 mm thick specimens oxidizing in pure steam during release. Arrows show the correction for volatilization of the specimen.

followed the initial rapid weight gain due to oxidation. The long-term weight loss rates were constant at all temperatures, and increased with temperature. The release data from high temperature anneals were corrected for fuel volatilization by assuming that: (i) the fission product concentration in the surface layer is the same as the average concentration in the specimen; and (ii) all fission product in the evaporated fuel is released (matrix-stripping approximation).

The specimen volatilization corrections are shown in Fig. 5 only for the longest anneal at 1600°C. For this combination, the correction reduces the observed fractional release by $\sim$20% for Ru and Mo, and, because of their smaller fractional releases, by $\sim$50% for Te and I. The upper points connected by the broken arrows in Fig. 5 represent f_{obs} and the lower points are the corrected values of f. The corrections to the other data points are not shown.

In addition to the largest volatility corrections, the experiments in steam at 1600°C show an apparent initial 'burst' of fission products that is not observed at any other temperature. This is indicated by the failure of the lines to pass through the origin of the 1600°C plot in Fig. 5. However, this observation depends on the accuracy of the data points at the shortest anneal time (8 min). Because the measurement of the single test is primarily responsible for the unusual behavior of the shortest-time points at 1600°C, there is a distinct possibility that the 'burst' phenomenon

is due to experimental error. The slopes of the lines in Fig. 5 at 1600°C are also affected by this potential source of error.

Fig. 6 compares the constant-stoichiometry results with those from the simultaneous-oxidation experiments. The points representing the latter are taken from the slopes of the lines in Fig. 5. The constant-stoichiometry points in Fig. 6 are the data in Fig. 3 for $UO_{2.20}$ with the fractional releases divided by $\sqrt{600}$, because the standardized anneal time for the data in the latter figure is 10 h.

The comparison in Fig. 6 shows that oxidation during release annealing effectively eliminates the temperature dependence of the release kinetics for Te, I and Ru. The two data sets for Mo are closer to each other than those of the other fission products, but it cannot be said that this element clearly behaves differently from the others during oxidative annealing. Even neglecting the variable-stoichiometry points at the highest temperature (lower left hand corner of the graphs in Fig. 6) because of the possible errors discussed above, there is a consistent suggestion in these data of a maximum release rate at ~ 1500°C.

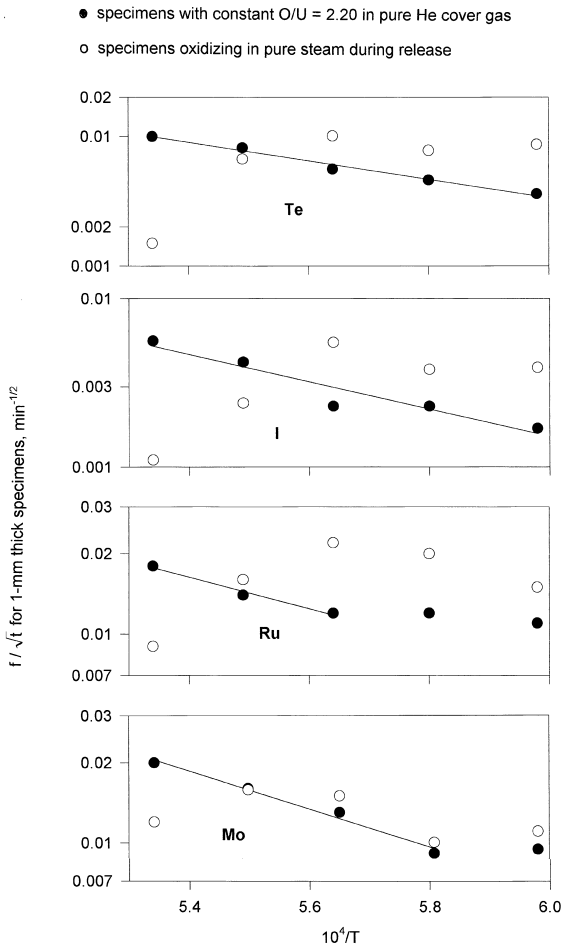

Fig. 6. Root-t scaled fractional releases for 1 mm thick specimens.

Although the variable-stoichiometry results show similar specimen-thickness dependence and the root-t behavior as the constant-stoichiometry data, the former exhibit features not previously observed in release from specimens with fixed O/U ratios. The non-Arrhenius behavior (or close-to-zero activation energy for release) and the departure from the root-t behavior at long anneal times occur even though the specimens spend $> 90\%$ of the anneal time at the equilibrium O/U ratio of ~ 2.20. Once oxidation is complete, the only difference in the two types of experiments is the ambient gas, which is pure He in the constant-stoichiometry experiments and pure steam in the variable stoichiometry tests. Aside from invoking a long-lasting 'memory effect' of oxidation of the specimen, no physical reason can be offered for the unusual behavior of the observed effects of simultaneous oxidation on fission product release. However, the effects observed are diametrically opposed to the way that the effect of oxidation on release is treated in mechanistic fission product release codes, in which release accelerates as fuel oxidation progresses. The data in this work show lower-than-expected releases at the longest times, not the shortest.

6. Discussion and conclusions

The principal objective of the investigation was to assess the effect of fuel stoichiometry on fission product release from trace-irradiated specimens whose morphology more closely resembles oxide fuel pellets than those used in previous investigations.

In stoichiometric UO_2, Te is by far the most easily-released, with the remaining species lower by factors of 4 to 10. When the O/U ratio is increased to 2.08 or 2.20, Ru and Mo releases jump by well over an order of magnitude, while those of I, Te, and Xe are limited to roughly twofold increases. These stoichiometry-driven effects are more modest than those ascribed to changes in fission-product diffusivities in earlier experimental works and considerably less dramatic than predicted by K&T's point-defect-based model. The very significant enhancement of Ru and Mo release that accompanies fuel oxidation is probably related to the higher volatility of the fully oxidized forms of these species compared to the low-vapor-pressure elemental states. However, the rapid release kinetics of Mo and Ru acquired when volatility limitations are removed means that their inherent mobility in the UO_{2+x} lattice is larger than the mobilities of completely-volatile species such as Xe and I.

The release augmentations due to fuel oxidation took place principally between exact stoichiometry and the first level of oxidation studied, $O/U = 2.08$. Between this state and $O/U = 2.20$, the release fractions were found to decrease as frequently as to increase.

A secondary goal of the research was to gain some understanding (beyond the level of the Booth model) of the mechanisms controlling the kinetics of release of the five fission products from oxidized fuel. Several release mechanisms incorporating both short-range and long-range diffusional processes were analyzed and compared to the experimental data. The theories had to fit both the observed specimen-size and root-t behavior. No model was found that satisfied both of these requirements. The grain boundary sweeping/grain boundary diffusion model could be fitted to reproduce the observed root-t behavior but not the observed specimen-size dependence of the release fractions in oxidized material. The lattice diffusion/dislocation diffusion combination could be fitted to reproduce the observed specimen-thickness dependence of the release fractions but it failed to predict root-t behavior. The lattice diffusion/in-pore gaseous diffusion model was ineffective in generating a size dependence of the release rates because gaseous diffusion coefficients are so much larger than solid-state diffusivities that transport in the existing open porosity could not be rate-limiting.

When the measured release fractions are placed on a common basis by time-scaling according to the root-t law and interpolating thickness effects to a hypothetical 1 mm thick specimen, two interesting features are revealed. The first is the existence of distinct breaks in the Arrhenius plots ($\log f$ vs. $1/T$) in oxidized fuel for all species except Xe. The second is the activation energies of the high-temperature portions of the Arrhenius plots. These ranged from 50–60 kcal/mol in $UO_{2.00}$ and 30–40 kcal/mol in $UO_{2.08}$ and $UO_{2.20}$. If interpreted in terms of the Booth model, the activation energies of the apparent Booth diffusion coefficients are twice as large as the values just cited for f. Such activation energies (100–120 kcal/mol for fission products in $UO_{2.00}$) are significantly larger than any previously reported in the literature.

The last topic investigated was simultaneous fuel oxidation and fission-product release. Since fuel oxidation occurred in times that were short compared to the anneal times for fission product release, the release fractions from the variable-stoichiometry tests (after correction for specimen evaporation) should have been comparable to those for the constant-stoichiometry tests using $UO_{2.20}$. However, they were not. The release rate activation energies for all fission products were nearly zero, long-term releases fell below the root-t behavior established in shorter anneals, and at the highest temperature investigated, apparent initial burst releases were observed.

Except for the replacement of helium ambient gas by pure steam, the simultaneous oxidation/release tests were essentially identical to the constant-stoichiometry experiments with $UO_{2.20}$. No quantitative explanation of the results summarized in the preceding paragraph can be offered at this time. It may be speculated that the rapid oxidation at the start of the anneal caused a disturbance in the UO_{2+x} lattice that enhanced fission product mobility in an athermal manner. The depressed release at long times may have been due to thermal annealing of the oxidation-induced structural damage.

Acknowledgements

This work was supported by the U.S. Department of Energy, Office of University and Science Educational Programs under grant number DE-FG07-9OER13033.

References

[1] R. Lindner, Hj. Matzke, Z. Naturforsch. 14a (1959) 582.
[2] W. Miekeley, F. Felix, J. Nucl. Mater. 42 (1972) 297.
[3] Hj. Matzke, Radiat. Eff. 53 (1980) 219.
[4] B.J. Lewis et al., Nucl. Technol. 92 (1990) 353.
[5] J.C. Killeen, J.A. Turnbull, An Experimental and Theoretical Treatment of the Release of ^{85}Kr from Hyperstoichiometric Uranium Dioxide, Proc. Workshop on Chemical Reactivity of Oxide Fuel and Fission Product Release, Glouscestershire, UK, 1987, p. 387.
[6] S.G. Prussin, D.R. Olander, P. Goubeault, D. Bayen, Release of Volatile Fission Products from UO_2, Proc. Am. Nucl. Soc. Meet. on Fission Product Behavior and Source Term Research, EPRI Report NP-4113-SR, 1985.
[7] S. Prussin, D.R. Olander, W. Lau, L. Hansson, J. Nucl. Mater. 154 (1988) 25.
[8] J.R. MacEwan, J.H. Stevens, J. Nucl. Mater. 11 (1964) 77.
[9] A. Mansouri, PhD thesis, University of California at Berkeley, 1995.
[10] G.T. Lawrence, J. Nucl. Mater. 71 (1978) 195.
[11] D. Cubiocciotti, J. Nucl. Mater. 154 (1988) 53.
[12] M.F. Notley, H. Manenc, Development of the ELSA release module, IPSN Note Technique SEMAR 96/44, 1996.
[13] B.J. Lewis et al., J. Nucl. Mater. 252 (1998) 235.
[14] I. Kaur, W. Gust, Grain and Interface Boundary Diffusion, Ziegler, Stuttgart, 1989.
[15] P.G. Shewmon, Diffusion in Solids, McGraw-Hill, New York, 1963.
[16] J.A. Turnbull, C.A. Friskney, J. Nucl. Mater. 58 (1975) 31.
[17] D.R. Olander, Adv. Ceram. 17 (1986) 271.
[18] U. El-Saied, D.R. Olander, J. Nucl. Mater. 207 (1993) 313.
[19] A.D. Le Claire, A. Rabinovitch, J. Phys. C 14 (1981) 3863.
[20] R.W. White, personal communication, 1996.
[21] T.J. Heames et al., VICTORIA: a Mechanistic Model of Radionuclide Behavior under Severe Accident Conditions NUREG/CR-5545, Rev. 1, 1992.